PAPER

High Performance OAM Communication Exploiting Port-Azimuth Effect of Loop Antennas

Hiroto OTSUKA[†], **Ryohei YAMAGISHI**[†], ***Student Members***, **Akira SAITOU**[†], ***Member***, **Hiroshi SUZUKI**[†], ***Fellow***, **Ryo ISHIKAWA**[†a)], ***Member***, ***and*** **Kazuhiko HONJO**[†], ***Fellow***

SUMMARY In this paper, we show that the orbital angular momentum (OAM) communication performance with a circular loop antenna array can be drastically improved by exploiting the port azimuth effect at the 5-GHz band. The received signal and interference powers are analytically derived with generalized Z-matrices and the perturbation method for short-range OAM communication. The resulting formulas show that the interference power can be drastically suppressed by selecting the proper combination of port azimuths. We also explain the mechanism behind the reduction in interference power. For the obtained port azimuth combination, the simulated and measured transmission isolations at 1 cm are better than 24.0 and 23.6 dB at 5.3 GHz, respectively. Furthermore, to estimate performance in 2×2 MIMO communication, constellations for 64-QAM are estimated. Measured EVMs are less than 3% where signals are clearly discriminated without any signal processing. For long-range OAM communication using paraboloids, the optimum port azimuth combination is estimated by monitoring the current distribution. For the obtained combination of the port azimuths, simulated and measured transmission isolations at 125 cm are better than 15.7 and 12.0 dB at 5.3 GHz, respectively. The measured isolation for short and long ranges are improved by 9.2 and 4.5 dB, respectively, compared with the data for the combination of the identical port azimuth.

key words: *loop antenna, orbital angular momentum, multiplexing*

1. Introduction

In order to improve the speed of or capacity for data transmission, various multiplexing methods have been investigated to improve the efficiency of frequency usage because the available frequency bands are valuable and finite resources. However, although efficiency is improved within the scope of the Shannon-Hartley theorem, exploiting those methods comes at the cost of exponential increases in power consumed. The multiple-input multiple-output (MIMO) communication method greatly reduces the power demands, but it requires complex signal processing for signal separation procedures. On the other hand, the orbital angular momentum (OAM) communication method also reduces the processing complexity by exploiting the orthogonality of the electromagnetic fields [1]–[7], where the carriers are spatially orthogonal because of their different orbital angular momentum. The angular momentum is represented by the rotating phase-front peculiar to OAM signaling. From the spatial orthogonality, multiplexing in the same frequency band is enabled, and the eigenmode transmission feature lessens both the power demands and signal processing complexity. Although applications for OAM communication are limited to fixed communication to maintain its spatial distribution of the OAM wave, OAM communication is anticipated to provide a novel dimension for multiplexing.

Thus, various methods have been proposed to generate the rather unique rotating phase front, such as array antennas with phase shifters [8]–[10] or phase-front transformation with spiral phase plates [11]–[15]. The former generates the rotating phase front by controlling the array factor with discretely shifted phase shifters. Signal processing is essential because all the transmitted carriers are received, but the complexity of the signal processing is expected to be somewhat mitigated. For the latter method, various pieces of equipment to receive only the desired carrier have been proposed, but these require a lot of space for items such as a beam splitter or a prism. Thus, a compact and simple configuration for OAM communication is desired, where only the desired carrier is received, as in eigenmode transmission.

A method to generate waves with a rotating phase front has been proposed by exploiting circular loop antennas [16], [17], where fairly pure single-mode waves are directly radiated from the antennas by setting the loop perimeter to be around an integral multiple of the wavelength. Due to the reciprocity for the transmitting and receiving antennas, the receiving antenna generally receives only the unique carrier of the mode. Thus, this method requires neither phase-transforming devices nor signal processing. The received power from the transmitting antenna of the same radius corresponds to the signal, and it is significantly larger than that from the transmitting antenna of a different radius caused by imperfect mode uniqueness. However, the latter substantially affects OAM communication performance, because it corresponds to the interference wave. Thus, to suppress undesired power, improvement of the mode uniqueness through the addition of a reflector plane was proposed [18]. Although that method is effective, the input impedances of the antennas must be drastically decreased in order to obtain excellent uniqueness. On the other hand, another method has been proposed to suppress undesired power by controlling the combination of port azimuths even where the mode uniqueness is rather poor [19]. This method can also be applied to a configuration with a reflector. However, although the obtained values of the azimuths have been explained, the mechanism regarding how the suppression is realized

Manuscript received December 11, 2018.
Manuscript revised May 8, 2019.
Manuscript publicized June 17, 2019.

[†]The authors are with the Department of Communication Engineering and Informatics, The University of Electro-Communications, Chofu-shi, 182-8585 Japan.
a) E-mail: r.ishikawa@uec.ac.jp

DOI: 10.1587/transcom.2018EBP3353

has not been reported, and applications to different configurations have proven difficult. Moreover, although the improvement of the signal-to-interference ratio (transmission isolation) has been explained, any relation to an index for actual communication, such as the signal-to-noise ratio or error-vector magnitude (EVM), remains to be explained.

In this paper, signal and interference powers are analytically clarified with the perturbation method for short-range OAM communication. With numerical calculation of the obtained formulas, the mechanism behind the suppression of undesired power is explained. In addition, the relation between the transmission isolation and EVM is measured with the fabricated arrays. Furthermore, it is demonstrated that signals for 64-quadrature amplitude modulation (QAM) are clearly discriminated without any signal processing for 2×2 MIMO communication.

2. Suppression of Undesired Transmission by Controlling Port-Azimuth

2.1 S-Matrices for Transmitting and Receiving Arrays

To suppress the interference by exploiting the port azimuth effect, the S-matrices for the loop antennas were analyzed with the generalized Z-matrix where the port azimuths were controlled. Figure 1 shows a configuration of analyzed transmitting and receiving arrays consisting of four-element loop antennas where their port azimuths are controlled. a_i, b_i, and ϕ_{ei} denote the loop radius, the conductor radius and the port azimuth for the i^{th} antenna, respectively. $d_{i,j}$ denotes the Z-component of the distance between the i^{th} and j^{th} antennas. The loop radii, the conductor radii, and the port azimuths are identical for the transmitting and receiving arrays. The port numbers are defined as 1 to 4 for the transmitting array, and 5 to 8 for the receiving array. Each port impedance (R_p) is assumed to be identical.

The current distribution for the i^{th} loop antenna can generally be Fourier-expanded, as shown in (1), where I_i^n denotes the current expansion coefficient for the n^{th} expansion order. Where the port azimuths are different, the n^{th}-order generalized Z-matrix $\mathbf{Z}^n$ is found as shown in (2), where $\boldsymbol{\zeta}^n$ is the generalized Z-matrix for the identical port azimuth. $\boldsymbol{\zeta}^n$ is given by (3)–(7) [17]. $\mathbf{A}^n$ is a matrix given by (8), which explains the effect of the port azimuth [20], [21]. $\mathbf{A}^n$ is the unit matrix for the identical port azimuth. The generalized Y-matrices, $\mathbf{Y}^n$ and $\boldsymbol{\xi}^n$, are obtained by the inverse matrix of $\mathbf{Z}^n$ and $\boldsymbol{\zeta}^n$, as shown in (9). When $\mathbf{Y}^{\pm n}$ is defined by (10), its matrix element is found with the generalized Y-matrix element for the identical port azimuth and the relative port azimuth for the i^{th} and j^{th} antennas, as shown in (11). As the i^{th} port current Ip_i is found by the sum for the expansion coefficients, the usual Y-matrix ($\mathbf{Y}^{\text{total}}$), which relates the voltage and current at the ports, is obtained as shown in (12). The S-matrix is obtained by the matrix transformation, as shown in (13), where E denotes the unit matrix. To suppress the interference, the S-matrix could be controlled by selecting the proper combination of the port azimuths, considering (10), (11) and (12).

$$I_i(\phi) = \sum_{n=-\infty}^{\infty} I_i^n e^{-jn(\phi-\phi_{ei})} \tag{1}$$

$$\mathbf{Z}^n = (\mathbf{A}^n)^{-1}\,\zeta^n\mathbf{A}^n \tag{2}$$

$$\begin{aligned}\zeta_{i,j}^n &= \zeta_{i,j}^{-n} \\ &= j\pi\eta_0\frac{1+\delta_{n,0}}{2}\left[\frac{K_{i,j}^{n-1}+K_{i,j}^{n+1}}{2}ka_j - \frac{n^2}{ka_i}\frac{K_{i,j}^n}{2}\right]\end{aligned} \tag{3}$$

$$\begin{aligned}K_{i,i}^{-n} &= K_{i,i}^n \\ &= \frac{1}{2\pi}\int_0^{2\pi}\left\{\frac{1}{2\pi}\int_0^{2\pi}\frac{e^{-jka_iR_{i,j}(\phi,\theta)}}{R_{i,i}(\phi,\theta)}e^{jn\phi}\mathrm{d}\phi\right\}\mathrm{d}\theta\end{aligned} \tag{4}$$

$$K_{i,j}^n = K_{i,j}^{-n} = \frac{1}{2\pi}\int_0^{2\pi}\frac{e^{-jka_iR_{i,j}(\phi,\theta)}}{R_{i,i}(\phi,\theta)}e^{jn\phi}\mathrm{d}\phi \tag{5}$$

$$R_{i,i}(\phi,\theta) = \left[4\sin^2\frac{\phi}{2} + 4\left(\frac{b_i}{a_i}\right)^2\sin^2\frac{\theta}{2}\right]^{1/2} \tag{6}$$

$$R_{i,j}(\phi,\theta) = \left[4\frac{a_j}{a_i}\sin^2\frac{\phi}{2} + \left(\frac{d_{i,j}}{a_i}\right)^2 + \left(\frac{a_j}{a_i}-1\right)^2\right]^{1/2} \tag{7}$$

$$[\mathbf{A}^n]_{i,j} = \delta_{i,j}e^{jn\phi_{ei}} \tag{8}$$

$$\mathbf{Y}^n = (\mathbf{Z}^n)^{-1} \qquad \xi^n = (\zeta^n)^{-1} \tag{9}$$

$$\mathbf{Y}^{\pm 0} \equiv \mathbf{Y}^0 \qquad \mathbf{Y}^{\pm n} \equiv \mathbf{Y}^n + \mathbf{Y}^{-n} \tag{10}$$

$$Y_{i,j}^{\pm n} = 2\xi_{i,j}^n\cos\left(n(\phi_{ej}-\phi_{ei})\right) \tag{11}$$

$$\begin{aligned}Ip_i = I_i(\phi_{ei}) &= \sum_{n=-\infty}^{\infty} I_i^n \\ &= \left[\sum_{n=0}^{\infty}\mathbf{Y}^{\pm n}\mathbf{V}\right]_i \equiv [\mathbf{Y}^{\text{total}}\mathbf{V}]_i\end{aligned} \tag{12}$$

$$\mathbf{S} = \left(\mathbf{E} + R_p\mathbf{Y}^{\text{total}}\right)^{-1}\cdot\left(\mathbf{E} - R_p\mathbf{Y}^{\text{total}}\right) \tag{13}$$

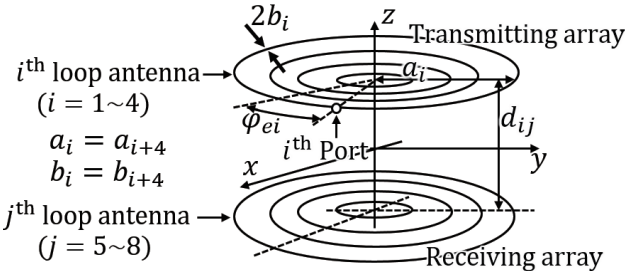

Fig. 1 Configuration of calculation for the shifted-port generalized Z-matrix.

2.2 Analysis for Port Currents

Whereas the interference wave is expressed using port azimuths, the formulas are quite complicated, and it is difficult to find an effective combination of port azimuths. To obtain simpler formulas, the generalized Z-matrices $\boldsymbol{\zeta}^n$ for the arrays of the identical port azimuth, all of which port-azimuths are zero, were numerically estimated with Mathematica™.

The conductor width was fixed at 0.4 mm. The distance between the transmitting and receiving arrays was selected to be 1 cm for the transmissions of the signal waves to be large enough. Return losses are determined mainly by loop radii. However, the transmission isolation is relatively independent of loop radii, where the return losses are good. Thus, loop radii were determined on condition that the port-azimuths are identical. Each order for the dominant current expansion coefficient was designed to be 1st, 2nd, 3rd and 4th for both the transmitting and receiving antennas. The target frequency was determined arbitrarily around 5.3 GHz. However, a substrate is not included for the numerical calculation, and the target frequency was increased by 10% for the loop radii to be similar to the fabricated ones. Thus, each loop radius was determined to be 8.57, 16.64, 24.67 and 32.68 mm, respectively, which adjusts the self-admittance such that each expansion order is almost a whole real number at 5.85 GHz, as explained in [17].

Table 1 shows the calculated absolute values of the normalized Y-matrix ($\mathbf{Y}^{\text{total}}$), where the normalizing port impedance (R_p) is 100 Ω. The calculated return losses were better than 10.3 dB at 5.85 GHz for all the antennas. The most dominant elements are self-admittances $Y^{\text{total}}_{i,i}$ and mutual admittances $Y^{\text{total}}_{i,i+4}$, and they are about 10 times larger than the other elements, as shown in Table 1. In addition, whereas their adjacent matrix elements are smaller than the most dominant elements, these are fairly larger than the other elements. In this case, the perturbation method can be exploited, where the most dominant elements and the adjacent elements correspond to the 0th order and the 1st order infinitesimals, respectively. In addition, the $Y^{\text{total}}_{i,i}$ are similar and around 1 because the port impedance was properly selected for the impedance matching. In addition, for $Y^{\text{total}}_{i,i+4}$, they are also similar. Furthermore, whereas $\mathbf{Y}^{\text{total}}$ is given by the sum of $\mathbf{Y}^{\pm n}$, the dominant contribution to $Y^{\text{total}}_{i,j}$ generally consists of the generalized Y-matrices for the dominant orders for both the i^{th} and j^{th} antennas. Since the dominant order for both the i^{th} and $(i+4)^{\text{th}}$ antennas is designed to be identical, $Y^{\text{total}}_{i,i}$ and $Y^{\text{total}}_{i,i+4}$, are almost identical to $Y^{\pm i}_{i,i}$ and $Y^{\pm i}_{i,i+4}$, as shown in Table 2.

Explained in physical terms, the current is almost that of the dominant order on the stimulated antenna, and the induced current is almost only on the antenna of the same radius. With the approximation, the induced port current on the receiving antenna for the adjacent order was analyzed, because the maximum undesired transmission has been that for the antenna [17]. Let the i^{th} antenna be stimulated by V_i. Where 1st order infinitesimals or more are neglected, the relations among the voltages and current can be concisely expressed as follows:

$$\begin{bmatrix} Ip_i \\ Ip_{i+4} \end{bmatrix} = \begin{bmatrix} Y^i_{i,i} & Y^i_{i,i+4} \\ Y^i_{i+4,i} & Y^i_{i+4,i+4} \end{bmatrix} \begin{bmatrix} V_i \\ -R_p Ip_{i+4} \end{bmatrix}. \tag{14}$$

The induced current is only at the port i and $i+4$, and the induced current is found as follows:

Table 1 Absolute values of normalized $\mathbf{Y}^{\text{total}}$ for identical port azimuths ($R_p = 100\,\Omega$, $f = 5.85$ GHz).

(a) $|Y^{\text{total}}_{11}|$ to $|Y^{\text{total}}_{48}|$

	1	2	3	4
1	5.8×10^{-1}	8.9×10^{-2}	2.3×10^{-2}	9.6×10^{-3}
2	8.9×10^{-2}	7.0×10^{-1}	1.0×10^{-1}	2.5×10^{-2}
3	2.3×10^{-2}	1.0×10^{-1}	1.0	1.2×10^{-1}
4	9.6×10^{-3}	2.5×10^{-2}	1.2×10^{-1}	1.3
5	6.0×10^{-1}	1.7×10^{-2}	5.8×10^{-3}	2.9×10^{-3}
6	1.7×10^{-2}	6.8×10^{-1}	3.9×10^{-2}	1.9×10^{-3}
7	5.8×10^{-3}	3.9×10^{-2}	9.2×10^{-1}	6.7×10^{-2}
8	2.9×10^{-3}	1.9×10^{-3}	6.7×10^{-2}	1.2

(b) $|Y^{\text{total}}_{15}|$ to $|Y^{\text{total}}_{88}|$

	5	6	7	8
1	6.0×10^{-1}	1.7×10^{-2}	5.8×10^{-3}	2.9×10^{-3}
2	1.7×10^{-2}	6.8×10^{-1}	3.9×10^{-2}	1.9×10^{-3}
3	5.8×10^{-3}	3.9×10^{-2}	9.2×10^{-1}	6.7×10^{-2}
4	2.9×10^{-3}	1.9×10^{-3}	6.7×10^{-2}	1.2
5	5.8×10^{-1}	8.9×10^{-2}	2.3×10^{-2}	9.6×10^{-3}
6	8.9×10^{-2}	7.0×10^{-1}	1.0×10^{-1}	2.5×10^{-2}
7	2.3×10^{-2}	1.0×10^{-1}	1.0	1.2×10^{-1}
8	9.6×10^{-3}	2.5×10^{-2}	1.2×10^{-1}	1.3

Table 2 Absolute values of normalized $Y^{\pm n}_{i,i+4}$ ($R_p = 100\,\Omega$, $f = 5.85$ GHz).

(a) 0th to ±2nd

	0	±1	±2
$\lvert Y^{\pm n}_{15}\rvert$	6.5×10^{-3}	5.9×10^{-1}	2.7×10^{-4}
$\lvert Y^{\pm n}_{26}\rvert$	5.8×10^{-3}	8.1×10^{-3}	6.7×10^{-1}
$\lvert Y^{\pm n}_{37}\rvert$	4.1×10^{-3}	8.0×10^{-3}	6.1×10^{-3}
$\lvert Y^{\pm n}_{48}\rvert$	3.5×10^{-3}	7.4×10^{-3}	8.2×10^{-3}

(b) 3rd to ±5th

	±3	±4	±5
$\lvert Y^{\pm n}_{15}\rvert$	1.8×10^{-4}	3.9×10^{-5}	8.9×10^{-6}
$\lvert Y^{\pm n}_{26}\rvert$	5.5×10^{-4}	6.6×10^{-4}	2.4×10^{-4}
$\lvert Y^{\pm n}_{37}\rvert$	9.1×10^{-1}	1.6×10^{-3}	1.1×10^{-3}
$\lvert Y^{\pm n}_{48}\rvert$	8.4×10^{-3}	1.2	6.1×10^{-3}

(c) ±6th, ±7th and total

	±6	±7	Total
$\lvert Y^{\pm n}_{15}\rvert$	2.2×10^{-6}	5.6×10^{-7}	6.0×10^{-1}
$\lvert Y^{\pm n}_{26}\rvert$	9.1×10^{-5}	3.7×10^{-5}	6.8×10^{-1}
$\lvert Y^{\pm n}_{37}\rvert$	4.8×10^{-4}	2.2×10^{-4}	9.2×10^{-1}
$\lvert Y^{\pm n}_{48}\rvert$	1.7×10^{-3}	7.7×10^{-4}	1.2

$$Ip_i = \left(R_p Y^i_{i,i} - \frac{\left(R_p Y^i_{i,i+4}\right)^2}{1 + R_p Y^i_{i,i}} \right) \frac{V_i}{R_p} \tag{15}$$

$$Ip_{i+4} = \frac{R_p Y^i_{i,i+4}}{1 + R_p Y^i_{i,i}} \frac{V_i}{R_p}. \tag{16}$$

With (15) and (16), the relations among the voltages and current can be concisely expressed as follows for the 1st order infinitesimals, where 2nd order infinitesimals or more are neglected:

$$\begin{bmatrix} Ip_i \\ Ip_j \\ Ip_{i+4} \\ Ip_{j+4} \end{bmatrix} = \begin{bmatrix} Y^i_{i,i} & Y^{\text{total}}_{i,j} & Y^i_{i,i+4} & Y^{\text{total}}_{i,j+4} \\ Y^{\text{total}}_{j,i} & Y^j_{j,j} & Y^{\text{total}}_{j,i+4} & Y^j_{j,j+4} \\ Y^i_{i+4,i} & Y^{\text{total}}_{i+4,j} & Y^i_{i+4,i+4} & Y^{\text{total}}_{i+4,j+4} \\ Y^{\text{total}}_{j+4,i} & Y^j_{j+4,j} & Y^{\text{total}}_{j+4,i+4} & Y^j_{j+4,j+4} \end{bmatrix} \begin{bmatrix} V_i \\ -R_p Ip_j \\ -R_p Ip_{i+4} \\ -R_p Ip_{j+4} \end{bmatrix} \quad (j = i \pm 1). \tag{17}$$

The induced currents of the 1st order infinitesimal are found as follows:

$$\begin{aligned} Ip_{j+4} = & \frac{V_i}{R_p \left(1 + R_p Y^j_{j,j} - \dfrac{\left(R_p Y^j_{j,j+4}\right)^2}{1 + R_p Y^j_{j,j}} \right)} \left[R_p Y^{\text{total}}_{i,j+4} \right. \\ & - \left(R_p^2 Y^{\text{total}}_{i,j}\right) \left(\frac{Y^i_{i,i+4}}{1 + R_p Y^i_{i,i}} - \frac{Y^j_{j,j+4}}{1 + R_p Y^j_{j,j}} \right) \\ & \left. + \frac{\left(R_p Y^i_{i,i+4}\right)\left(R_p Y^{\text{total}}_{i,j+4}\right)\left(R_p Y^j_{j,j+4}\right)}{\left(1 + R_p Y^i_{i,i}\right)\left(1 + R_p Y^j_{j,j}\right)} \right]. \end{aligned} \tag{18}$$

The received power for the k^{th} receiving antenna (P_k) is given as follows:

$$P_k = \frac{1}{2} R_p |Ip_k|^2 \qquad (k = 5, 6, 7, 8). \tag{19}$$

Thus, each power for the signal and interference can be estimated with (16) and (18). For the interference, the induced current consists of four terms, which may be interpreted to correspond to the paths shown in Fig. 2.

Whereas the induced current for the interference can be reduced by estimating various combinations of the port azimuths, we estimated a promising combination considering the features of (18). Figure 3(a) shows the contributions of the four terms for Ip_8 when the 3rd port was stimulated, where all the port azimuths are identical. The 4th term is much smaller than the other three terms. Since the phases for the 2nd and 3rd terms are similar, the sum shown in pink intensifies. As a result, when the phase difference of the 2nd and 3rd term is controlled to be π, these mutually negate, because the absolute values of $Y^{\pm i}_{i,i}$ and $Y^{\pm j}_{j,j}$ are similar. For i and j, one is odd and the other is even. Thus, with (11), the differences for their port azimuths are determined to be π for the 2nd and 3rd terms to mutually negate. In this case, the combination of the port azimuths, defined as DEG-A, is as follows:

$$\begin{aligned} \phi_{ei} &= 0^\circ \quad (i = 1, 2, 3, 4), \\ \phi_{ej} &= 180^\circ \quad (j = 5, 6, 7, 8). \end{aligned} \tag{20}$$

To verify the obtained results, the transmission characteristics were numerically estimated for a distance of 1 cm, as shown in Fig. 4. Except the combination of the port azimuth, the dimensions of the loop antenna arrays are identical. As expected, undesired transmission to the adjacent receiving antenna is sharply reduced around the designed 5.85 GHz.

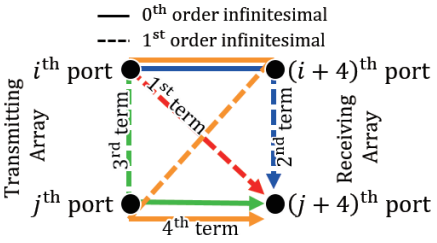

Fig. 2 Terms of (18).

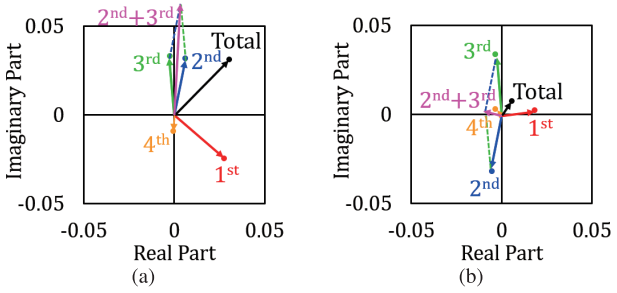

Fig. 3 Values of each term in (18) for Ip_8, when . (a) All port azimuths are identical. (b) Receiving port azimuths are 180°.

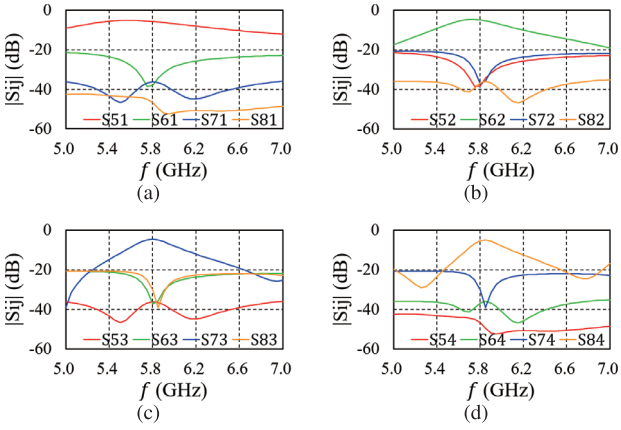

Fig. 4 Calculated transmission characteristics where port azimuths for the receiving array are rotated by 180 degrees. (a) 1st port is stimulated. (b) 2nd port is stimulated. (c) 3rd port is stimulated. And (d) 4th port is stimulated.

For example, S_{61} was remarkably reduced from −23.0 to −34.4 dB by controlling the combination. For the performance index, the transmission isolation IT has been defined as follows [17]:

$$\begin{aligned} \text{IT [dB]} = \min_i \{ \min_j (& S_{i+4,i} \text{ [dB]} - S_{j,i} \text{ [dB]}) \} \\ & (i = 1, 2, 3, 4 \quad j = 5, 6, 7, 8). \end{aligned} \tag{21}$$

$S_{i+4,i}$ and $S_{j,i}$ correspond to the transmissions for the signal and interference waves, respectively, where antenna i is stimulated. Thus, the transmission isolation corresponds to the worst value of signal to interference ratio for the four communication channels, which is defined at each frequency. The calculated IT for DEG-A is more than 28.4 dB at 5.85 GHz, which is improved by 11.1 dB compared to the arrays for

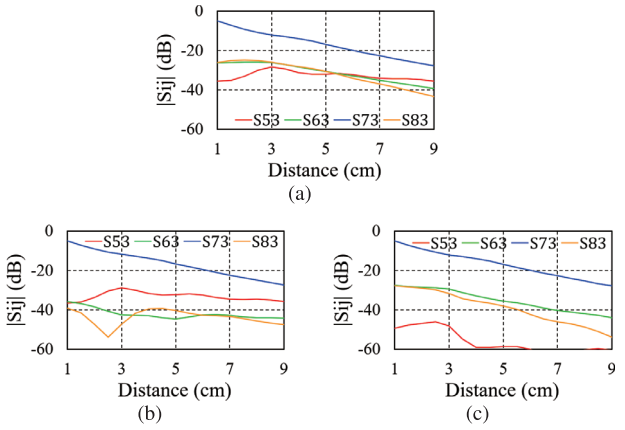

Fig. 5 Calculated transmission coefficients where . (a) All port azimuths are identical. (b) DEG-A. (c) DEG-B.

the identical port azimuth [17]. This result demonstrates that port azimuth control is quite effective at improving the OAM communication performance.

Since the Y-matrix values change by the distance between the arrays, the effects of the communication distance on the transmissions were also estimated. Another combination for long-range OAM communication (DEG-B), explained in Sect. 3, was included. The dimensions of the loop antenna arrays are identical. The combination of DEG-B is as follows:

$$\begin{aligned} \phi_{e1} = \phi_{e5} = 0^\circ, \quad \phi_{e2} = \phi_{e6} = 60^\circ, \\ \phi_{e3} = \phi_{e7} = 96^\circ, \quad \phi_{e4} = \phi_{e8} = 121^\circ. \end{aligned} \tag{22}$$

The communication distances were varied, from 1 to 9 cm. Figure 5 shows the calculated transmission, where the 3rd port was stimulated at 5.85 GHz. The maximum transmission is always S_{73}, which corresponds to the signal. For the arrays of the identical port azimuths, the second largest transmissions are S_{83} and S_{63}, up to 5 cm, as shown in Fig. 5(a). These are undesired transmissions, and the dominant orders (2nd and 4th) for the 6th and 8th receiving antennas are adjacent to that (3rd) of the transmitting antenna. However, at the greater distance, the undesired transmission to the smallest receiving antenna (S_{53}) becomes the largest. This can be explained by the fact that the smallest antenna effectively receives the 1st-order radiation mode generated by the 1st-order current expansion coefficient, and the 1st-order radiation mode expands the least. On the other hand, for the combination of DEG-A, whereas S_{53} is almost identical, undesired transmissions to the antenna of the adjacent orders are drastically reduced, up to 9 cm, as shown in Fig. 5(b). As a result, the combination of DEG-A is superior to that of the identical azimuths, over which S_{53} becomes the largest for that of the identical azimuths. For the combination of DEG-B, whereas S_{83} and S_{63} are similar to that of the identical azimuths, S_{53} is remarkably reduced, as shown in Fig. 5(c), and the combination of DEG-B may be said to be more suitable for distances greater than 5 cm.

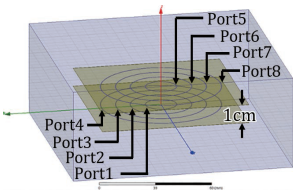

Fig. 6 Configuration of short-range simulation.

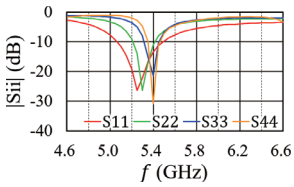

Fig. 7 Return losses of simulated loop antennas.

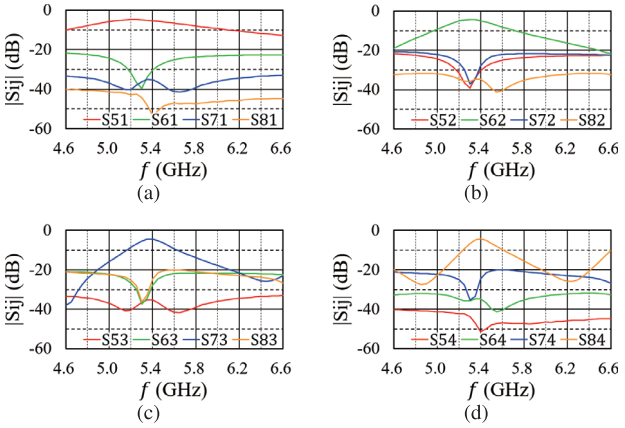

Fig. 8 Simulated transmission characteristics where port azimuths are DEG-A. (a) 1st port is stimulated. (b) 2nd port is stimulated. (c) 3rd port is stimulated. And (d) 4th port is stimulated.

2.3 Simulated Performance for Short-Range OAM Communication

To verify that the combination of DEG-A is effective for short-range OAM communication, characteristics were simulated with HFSS™ [22]. Figure 6 shows a simulated configuration. The distance between the transmitting and receiving array is 1 cm, and the conductor widths are fixed at 0.4 mm. The obtained loop radii were 8.4, 16.5, 24.4 and 32.5 mm, respectively. The loop antenna arrays were concentrically laid out on a 0.1-mm-thick FR-4 substrate ($\epsilon_r = 4.8$, $\tan\delta = 0.01$). The port impedances are fixed at 100 Ω, where the simulated return losses are better than 5.0 dB at 5.3 GHz, as shown in Fig. 7. Figure 8 shows the simulated transmission for DEG-A. As is the case with the numerical analysis, the transmissions between the transmitting and receiving antennas of the same radius are always the maximum, and undesired transmissions to the receiving antennas of the adjacent order are sharply reduced around the resonant frequency. As a result, the transmission isolation is reduced to a maximum of 24.0 dB at 5.3 GHz.

2.4 Measured Performance for Short-Range OAM Communication

To verify the simulated results, antennas for the simulated configuration were fabricated, as shown in Fig. 9. The distance between the arrays was 1 cm. Baluns are integrated

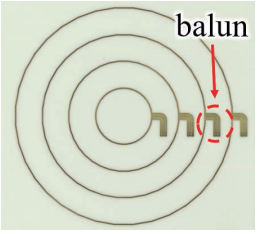

Fig. 9 Fabricated loop antenna array for short-range.

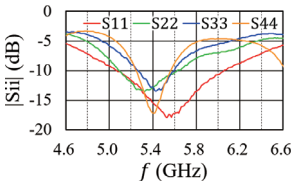

Fig. 10 Measured return loss of DEG-A.

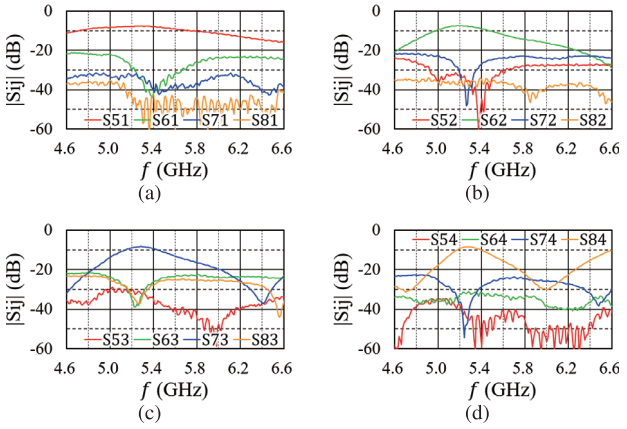

Fig. 11 Measured transmission characteristics where port azimuths are DEG-A. (a) 1st port is stimulated. (b) 2nd port is stimulated. (c) 3rd port is stimulated. And (d) 4th port is stimulated.

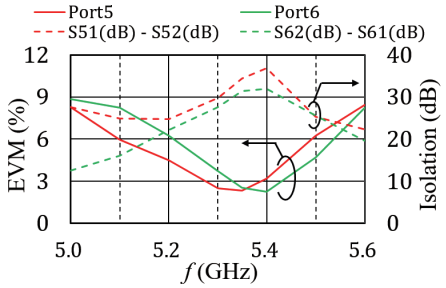

Fig. 12 Relation between EVM and isolation.

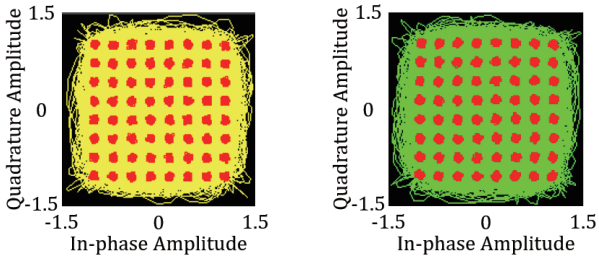

Fig. 13 Signal space diagrams of receiving 64-QAM signals at 5.35 GHz. (a) At the 5th port. (b) At the 6th port.

for impedance transformation between the input impedances of about 100 Ω and the port impedance of 50 Ω, where the measured return losses are better than 10.9 dB at 5.3 GHz, as shown in Fig. 10. Figure 11 shows the measured transmission. Undesired transmissions are also sharply reduced around the resonant frequency. The measured transmission isolation is more than 23.6 dB at 5.3 GHz, which is better by 9.2 dB than that reported in [17]. Thus, port azimuth control is indeed effective for short-range OAM communication.

2.5 Measured Performance for Short-Range LOS-MIMO Communication

Transmission isolation is considered the most important index of OAM communication performance, because it expresses the power ratio for the signal and interference. Nevertheless, it is not a direct performance index, such as the signal-to-noise ratio (S/N) or the error-vector magnitude (EVM). Thus, to examine the relations between transmission isolation and EVM, characteristics for line-of-sight MIMO (LOS-MIMO) communication were measured with a pair of vector signal generators (N5172B) and a vector signal analyzer (MSOS804) from Keysight Technologies. The distance between the arrays was 1 cm. Since only two input ports were available, transmitting antennas 1 and 2 were connected to the input ports, and receiving antennas 5 and 6 were connected to the analyzer. The other ports were terminated by 50 Ω. The symbol rate was 75M Symbols/s, and the roll-off factor was 0.5. The modulation scheme was 64-QAM. No MIMO signal processing was included. Figure 12 shows the frequency characteristics for EVM and the isolation. The transmission isolation is closely correlated with EVM, and EVM becomes less than 3% where the transmission isolation is higher than 30 dB. Figure 13 shows the signal space diagrams of the received 64-QAM signals. The signal constellations at 5.35 GHz are clearly discriminated for both channels by virtue of the lower EVM. On the other hand, the signal constellations were not discriminated at 5.6 GHz, where the transmission isolation is around 20 dB.

3. Assessment for Long-Range OAM Communication

3.1 Simulated Performance for Long-Range OAM Communication

Analysis with the perturbation method is not applied for long-range OAM communication, as shown in Sect. 2.2. In addition, as the paraboloids are utilized to collimate the expanding OAM wave, as shown in Fig. 14, analysis with the generalized Z-matrices is also impossible. However, the aim of the analysis was for undesired port currents to be suppressed, which can be estimated with a simulator. Thus, by varying the combination of the port azimuths, undesired port currents were repeatedly simulated for the configuration shown in Fig. 14. The distance between the transmitting and receiving array is 125 cm. The radius and the focal length of the paraboloid are 30 cm and 21.5 cm, respectively. The radius was smaller than the radius used for measurement shown below because of the limit of the available memory size. To confirm the potential, the transmission isolation was

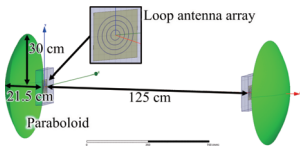

Fig. 14 Configuration of long-range simulation.

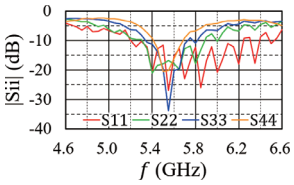

Fig. 15 Return losses of simulated loop antennas.

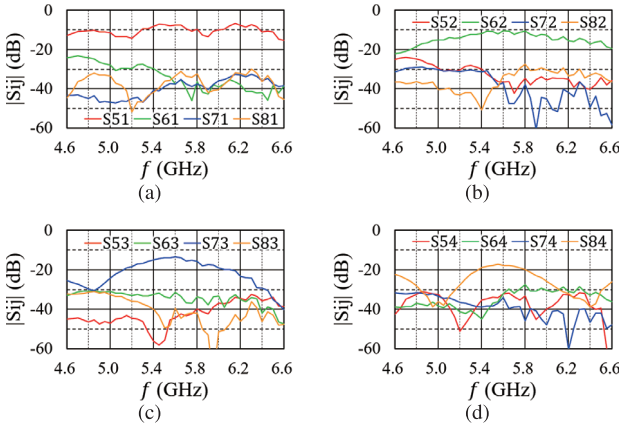

Fig. 16 Simulated transmission characteristics where port azimuths are DEG-B. (a) 1st port is stimulated. (b) 2nd port is stimulated. (c) 3rd port is stimulated. (d) 4th port is stimulated.

estimated. The arrays are located in the focal plane. The loop radii, conductor radii, and the substrate for the antennas are identical to those for the short-range OAM communication, shown in Sect. 2.3. The obtained combination of the port azimuths, defined as DEG-B, is as follows:

$$\begin{aligned} \phi_{e1} = \phi_{e5} = 0^\circ, \quad \phi_{e2} = \phi_{e6} = 60^\circ, \\ \phi_{e3} = \phi_{e7} = 96^\circ, \quad \phi_{e4} = \phi_{e8} = 121^\circ. \end{aligned} \tag{23}$$

The simulated return losses were better than 5.5 dB at 5.3 GHz, as shown in Fig. 15. Figure 16 shows the simulated transmission characteristics for DEG-B. The transmissions between the antennas of the same radii are the maximum around 5.3 GHz. The transmission S_{84} is the smallest, where the transmission is mediated by the highest 4^{th}-order mode fields for the magnetic quantum number. This can be explained by the diffraction characteristics for the mode order [17]. Undesired transmissions were reduced and the transmission isolation was better than 15.7 dB at 5.3 GHz.

3.2 Measured Performance for Long-Range OAM Communication

When we first measured the transmission for a long range, remarkably jagged frequency characteristics were observed. Since interference by multiple paths was a concern, time-domain measurements were implemented. Figure 17 shows the schematic configuration and the measured time-domain transmission characteristics. Three peaks were confirmed. By examining the relation between the distance and the delays, these peaks were identified to correspond to paths A, B_1, B_2 and C, as shown in the figure. Since the paraboloids are used for collimating the radiated fields, path C is the desired path. Thus, time-gating was implemented to extract the transmission from 11 to 18 ns to extract only the data for path C.

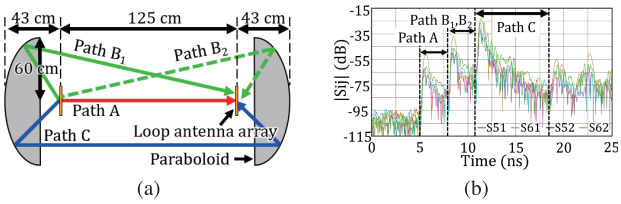

Fig. 17 (a) Configuration for multi-path. (b) Time domain waveform for multi-path.

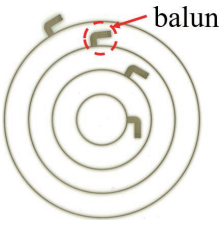

Fig. 18 Fabricated loop antenna array for long range.

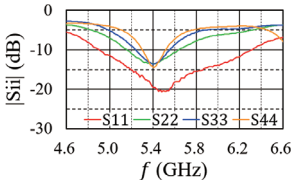

Fig. 19 Measured return loss for DEG-B.

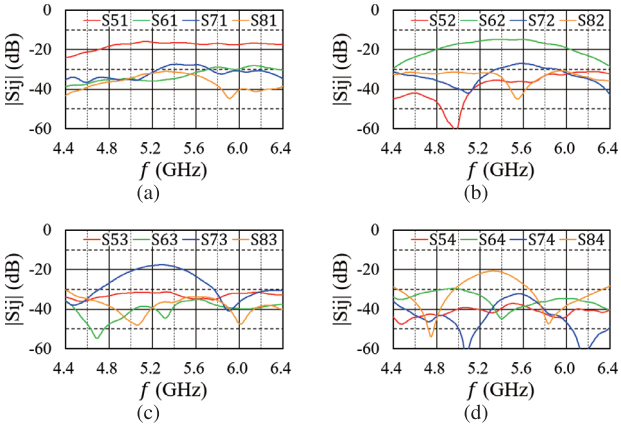

Fig. 20 Measured transmission characteristics where port azimuths are DEG-B. (a) 1st port is stimulated. (b) 2nd port is stimulated. (c) 3rd port is stimulated. (d) 4th port is stimulated.

The arrays of the simulated configuration were fabricated as shown in Fig. 18. The measured return losses were better than 10.0 dB at 5.3 GHz, as shown in Fig. 19. The distance between the transmitting and receiving arrays was 125 cm. The radius and the focal length of the paraboloid were 60 and 43 cm, respectively. The arrays are located in the focal plane, and the paraboloids and the arrays were carefully aligned with a laser for the central axes to coincide. Figure 20 shows the measured transmission characteristics. Undesired transmissions were reduced around the point where the return losses were good. The measured isolation was more than 12.0 dB at 5.3 GHz and improved by 4.2 dB compared with identical port azimuths [17].

4. Conclusion

Performance of OAM communication with circular loop antennas was drastically improved by exploiting the port azimuth effect in the 5-GHz band. The received signal and interference power were analytically derived with the generalized Z-matrices and the perturbation method for short-range OAM communication. With numerical calculation of the obtained formulas, the interference power was shown to be markedly suppressed by selecting the proper combination of port azimuths. The mechanism behind the suppressed interference power was also explained. For the obtained port azimuth combination, the simulated and measured transmission isolations at 1 cm were better than 24.0 and 23.6 dB at 5.3 GHz, respectively. Furthermore, to estimate performance in 2×2 MIMO communication, constellations for 64-QAM were estimated. Measured EVMs were less than 3%, where signals were clearly discriminated without any signal processing. For long-range OAM communication using paraboloids, the optimum port azimuth combination was estimated by monitoring the current distribution. The obtained combination of port azimuths yielded, for the array separation of 125 cm, simulated and measured transmission isolations of better than 15.7 and 12.0 dB at 5.3 GHz, respectively. The measured isolation for short and long ranges were improved by 9.2 and 4.2 dB, compared with the data for the combination of the identical port azimuth.

Acknowledgments

This research and development work was supported by the MIC/SCOPE #175003001.

References

[1] L. Allen, M.W. Beijersbergen, R.J.C. Spreeuw, and J.P. Woerdman, "Orbital angular momentum of light and the transformation of Laguerre-Gaussian laser modes," Phys. Rev. A., vol.45, no.11, pp.8185–8189, June 1992.

[2] H. He, M.E.J. Friese, N.R. Heckenberg, and H. Rubinsztein-Dunlop, "Direct observation of transfer of angular momentum to absorptive particles from a laser beam with a phase singularity," Phys. Rev. Lett., vol.75, no.5, pp.826–829, July 1995.

[3] S. Franke-Arnold, L. Allen, and M. Padgett, "Advances in optical angular momentum," Laser Photon. Rev., vol.2, no.4, pp.299–313, July 2008.

[4] J. Wang, J.-Y. Yang, I.M. Fazal, N. Ahmed, Y. Yan, H. Huang, Y. Ren, Y. Yue, S. Dolinar, M. Tur, and A.E. Willner, "Terabit free-space data transmission employing orbital angular momentum multiplexing," Nature Photon., vol.6, pp.488–496, July 2012.

[5] F. Tamburini, E. Mari, A. Sponselli, B. Thidé, A. Bianchini, and F. Romanato, "Encoding many channels on the same frequency through radio vorticity: First experimental test," New J. Phys., vol.14, pp.1–17, March 2012.

[6] D. Lee, H. Sasaki, H. Fukumoto, K. Hiraga, and T. Nakagawa, "Orbital angular momentum multiplexing: An enabler of a new era of wireless communications," IEICE Trans. Commun., vol.E100-B, no.7, pp.1044–1063, July 2017.

[7] S.M. Mohammadi, L.K.S. Daldorff, J.E.S. Bergman, R.L. Karlsson, B. Thidé, K. Forozesh, T.D. Carozzi, and B. Isham, "Orbital Angular momentum in Radio- A system study," IEEE Trans. Antennas Propag., vol.58, no.2, pp.565–572, Feb. 2010.

[8] Q. Bai, A. Tennant, and B. Allen, "Experimental circular phased array for generating OAM radio beams," Electron. Lett., vol.50, no.20, pp.1414–1415, 2014.

[9] G. Xie, Y. Yan, Z. Zhao, L. Li, Y. Ren, N. Ahmed, A.J. Willner, C. Bao, Z. Wang, C. Liu, N. Ashrafi, S.A. Talwar, S. Sajuyigbe, M. Tur, A.F. Molisch, and A.E. Willner, "Tunable generation and angular steering of a MillimeterWave orbital-angular-momentum beam using differential time delays in a circular antenna array," IEEE International Conf. Commun., 2016.

[10] K. Liu, H. Liu, Y. Qin, Y. Cheng, S. Wang, X. Li, and H. Wang, "Generation of OAM beams using phased array in the microwave band," IEEE Trans. Antennas Propag., vol.64, no.9, pp.3850–3857, Sept. 2016.

[11] W. Wei, K. Mahdjoubi, C. Brousseau, and O. Emile, "Horn antennas for generating radio waves bearing orbital angular momentum by using spiral phase plate," IET Microw. Ant. & Propag., vol.10, no.13, pp.1420–1427, 2016.

[12] Y. Chen, S. Zheng, Y. Li, X. Hui, X. Jin, H. Chi, and X. Zhang, "A flat-lensed spiral phase plate based on phase-shifting surface for generation of millimeter-wave OAM beam," IEEE Antennas Wireless Propag. Lett., vol.15, pp.1156–1158, 2016.

[13] Y. Yan, G. Xie, M.P.J. Lavery, H. Huang, N. Ahmed, C. Bao, Y. Ren, Y. Cao, L. Li, Z. Zhao, A.F. Molisch, M. Tur, M.J. Padgett, and A.E. Willner, "High-capacity millimeter-wave communications with orbital angular momentum multiplexing," Nat. Commun., vol.5, 4876, Sept. 2014.

[14] X. Hui, S. Zheng, Y. Hu, C. Xu, X. Jin, H. Chi, and X. Zhang, "Ultralow reflectivity spiral phase plate for generation of millimeter-wave OAM beam," IEEE Antennas Wireless Propag. Lett., vol.14, pp.966–969, 2015.

[15] Y. Yan, L. Li, Z. Zhao, G. Xie, Z. Wang, Y. Ren, N. Ahmed, S. Sajuyigbe, S. Talwar, M. Tur, N. Ashrafi, S. Ashrafi, A.F. Molisch, and A.E. Willner, "32-Gbit/s 60-GHz millimeter-wave wireless communication using orbital angular momentum and polarization multiplexing," IEEE ICC, 2016.

[16] A. Saitou, R. Ishikawa, and K. Honjo, "4-value multiplexing orbital-angular-momentum communication scheme using loop-antenna arrays," Asia Pacific Microw. Conf., Dec. 2016.

[17] H. Otsuka, R. Yamagishi, A. Saitou, R. Ishikawa, and K. Honjo, "Analytical and measured estimation for 4-value multiplexing OAM communication using loop array antennas," European Microw. Conf., Oct. 2017.

[18] R. Yamagishi, H. Otsuka, A. Saitou, R. Ishikawa, and K. Honjo, "Improvement of mode uniqueness for OAM communication using loop array with reflector plane," Asia Pacific Microw. Conf., Nov. 2017.

[19] H. Otsuka, R. Yamagishi, A. Saitou, R. Ishikawa, and K. Honjo, "High performance OAM communication using loop antennas optimized for port azimuths," Asia Pacific Microw. Conf., Nov. 2017.

[20] A. Saitou, H. Otsuka, R. Yamagishi, R. Ishikawa, and K. Honjo, "Analysis on doubling multiplicity for OAM communication using loop antenna arrays," Asia Pacific Microw. Conf., Nov. 2017.

[21] S. Ito, N. Inagaki, and T. Sekiguchi, "An investigation of the array of circular-loop antennas," IEEE Antennas Wireless Propag., vol.19, no.4, pp.2956–2963, July 1971.

[22] ANSYS, "ANSYS HFSS," https://www.ansys.com/Products/Electronics/ANSYS-HFSS

Hiroto Otsuka received the B.E. degree in information and communication engineering from the University of Electro-Communications, Tokyo, Japan, in 2017, and is currently working toward the M.E. degreeat the University of Electro-Communications, Tokyo, Japan.

Ryohei Yamagishi received the B.E. degree in information and communication engineering from the University of Electro-Communications, Tokyo, Japan, in 2017, and is currently working toward the M.E. degreeat the University of Electro-Communications, Tokyo, Japan.

Akira Saitou received his B.E. and M.E. degrees in applied physics from the University of Tokyo in Tokyo, Japan, in 1975 and 1977, respectively, and his D.E. degree in Information and Communication Engineering from the University of Electro-Communications in Tokyo, Japan, in 2008. From 1977 to 2002, he was employed at NEC Corporation to develop GaAs FETs and MMICs for microwave and millimeter-wave communication. From 2002–2009, he worked for YKC Corporation to develop microwave circuits and antennas for short-range wireless interfaces. In 2009, he joined the University of Electro-Communications as a guest professor in the Advanced Wireless Communication Research Center.

Hiroshi Suzuki received the B.S. degree in electrical engineering, the M.S. degree in physical electronics, and the Dr. Eng. Degree in electrical and electronics engineering, all from the Tokyo Institute of Technology, Tokyo, in 1972, 1974, and 1986, respectively. He joined the Electrical Communication Laboratories, Nippon Telegraph and Telephone Corporation (NTT), Japan, in 1974. He was engaged in research on devices in millimeter-wave regions. Since 1978, he has been engaged in fundamental and developmental researchers on digital mobile communication systems. He was an Executive Research Engineer in the Research and Development Department, NTT Mobile Communications Network, Inc. (NTT DoCoMo) from 1992 to 1996. In September 1996, he became Professor at the Tokyo Institute of Technology, and in April 2015 he became Professor Emeritus of Tokyo Institute of Technology. Since 2016 he has been Guest Professor of Advanced Wireless & Communication Research Center (AWCC), the University of Electro-Communications. He is currently interested in various applications of the adaptive signal processing to radio signal transmission: adaptive arrays, multiuser detection, interference canceling, and MIMO-OFDM, OAM for future advanced multiple access and relay radio communication systems. Prof. Suzuki is a fellow of the Institute of Electronics, Information, and Communication Engineers (IEICE) of Japan, and a life member of IEEE. He received the Paper Award from the IEICE in 1995, 2007, 2009 and 2012, Best Paper Award from EuWiT in 2009, the award of IEICE Fellow in 2006, and IEICE Achievement Award in 2009.

Ryo Ishikawa received the B.E., M.E., and D.E. degrees in electronic engineering from Tohoku University, Sendai, Japan, in 1996, 1998, and 2001, respectively. In 2001, he joined the Research Institute of Electrical Communication, Tohoku University, Sendai, Japan. In 2003, he joined the University of Electro-Communications, Tokyo, Japan. His research interest is the development of microwave compound semiconductor devices and related techniques. Dr. Ishikawa is a member of the Japan Society of Applied Physics. He was the recipient of the 1999 Young Scientist Award for the Presentation of an Excellent Paper of the Tohoku Chapter, Japan Society of Applied Physics.

Kazuhiko Honjo received the B.E. degree from the University of Electro-Communications, Tokyo, in 1974, and the M.E. and D.E. degrees in electronic engineering from the Tokyo Institute of Technology, Tokyo, in 1976 and 1983, respectively. From 1976 to 2001, he worked for NEC Corporation, Kawasaki, Japan. In 2001, he joined the University of Electro-Communications as a professor in the Information and Communication Engineering Department. He has been involved in research and development of high-power/broadband/low-distortion microwave amplifiers, MMICs, HBT device and processing technology, miniature broadband microwave antennas and FDTD electro-magnetic wave and device coanalysis. Prof. Honjo received both the 1983 Microwave Prize and the 1988 Microwave Prize granted by the IEEE Microwave Theory and Techniques Society. He also received the 1980 Young Engineer Award, and the 1999 Electronics Award both presented by the Institute of Electrical, Information and Communication Engineers (IEICE), Japan. He is Fellow of IEEE.